Permafrost and Periglacial Processes

WILEY

RESEARCH ARTICLE OPEN ACCESS

Nearshore Hydrodynamics and Sediment Dispersal Along Eroding Permafrost Coasts—Insights From Acoustic Doppler Current Profiler Measurements Around Herschel Island–Qikiqtaruk (Yukon, Canada)

Justus Gimsa[1,2] | Michael Fritz[2] | Hugues Lantuit[1,2]

[1]Institute of Geosciences, University of Potsdam, Potsdam, Germany | [2]Permafrost Research Section, Alfred Wegener Institute Helmholtz Centre for Polar and Marine Research, Potsdam, Germany

Correspondence: Justus Gimsa (justus.gimsa@awi.de)

Received: 7 February 2024 | **Revised:** 10 July 2024 | **Accepted:** 2 November 2024

Funding: This work was supported by the European Union Horizon 2020 (773421).

Keywords: Acoustic Doppler Current Profiler | Arctic Ocean | Beaufort Sea | Nearshore Sediment Transport | Permafrost Coasts

ABSTRACT

Permafrost coasts are eroding at an accelerating pace, delivering vast amounts of sediments, organic matter, nutrients, and pollutants into the Arctic Ocean. These fluxes play a crucial role in the coastal biogeochemical cycle, yet their magnitude, as well as the trajectory and fate of the eroded material, is largely unknown. Direct observations of hydrodynamics in the Arctic nearshore zone are needed to overcome this issue, but these are challenging and scarce. Here, we report on direct current measurements performed in the nearshore zone. We deployed two Acoustic Doppler Current Profilers (ADCP) in 7- and 12-m water depth close to Herschel Island–Qikiqtaruk Yukon, Canada, to measure current velocities and directions throughout the water column. The data show that the currents change on a synoptic scale based on meteo-oceanographic forcing. During storms, these currents exceed the threshold of bottom sediment remobilization. The mobilization potential in the nearshore zone is therefore primarily related to wind forcing but can be strongly diminished by the presence of sea ice. These observations have implications for the future state of the Arctic nearshore zone, because larger fetches and a longer open water season could enhance sediment mobilization and dispersal.

1 | Introduction

The Arctic coastline is more than 400,000 km long. This is about a third of the world's coastline [1]. Much of this coastline is frozen as permafrost (sediment, soil and rock that is frozen for more than two consecutive years). These coasts are often rich in ice (i.e., ground ice) and therefore highly vulnerable to thaw and erosional processes [2, 3]. Increasing air and water temperatures, together with sea ice shrinkage and enhanced ocean waves and storm events, lead to higher coastal erosion rates of the ice-bound sedimentary material [4, 5]. Erosion rates are projected to increase by a factor of 2 to 3 under the SSP5-8.5 warming scenario [6, 7]. The associated land-loss threatens local infrastructure, as well as cultural and archeological sites. The eroded matter entering the sea can also be rich in carbon and nutrients and has the potential to alter the nearshore biogeochemistry [8]. Organic carbon that enters the sea can be rapidly released as greenhouse gas [9], potentially fuelling further climate warming. Next to CO_2 production from eroded organic carbon on land and in the nearshore zone [9, 10], another share gets transported offshore or alongshore and is buried in nearshore or offshore sediment sinks [11, 12]. Remote sensing of Arctic coastal zones shows that large plumes of sediment associated with coastal erosion can drift over hundreds of kilometers [13, 14].

The pathways of eroded coastal sediment are critical, as studies have highlighted the importance of the nearshore zone for the degradation of this previously freeze-locked matter [12, 15–17]. This critical nearshore zone (< 20-m water depth) of the Arctic Ocean accounts for around 20% of the size of its shelf [8]. The Arctic Ocean coastal current dynamics are poorly understood, because landfast-ice threatens traditional sea-floor mooring systems in shallow water, which leaves a paucity in directional nearshore currents and wave measurements. Although measurements of Arctic currents exist [18, 19], they are usually limited to depths greater than 20 m, and the shallow nearshore zone along eroding coasts has been the scope of very few studies [20]. The aim of this paper is to provide direct measurements of the direction and velocity of coastal currents in the upper and lower water column in the nearshore zone of Herschel Island–Qikiqtaruk, where high rates of coastal erosion of up to 22 m/year and retrogressive thaw slumps discharge large amounts of terrestrial material into the nearshore environment [21–23]. Specifically, we aim to relate the nature of the observed currents to driving environmental forces and to bring this into the context of sediment transport and resuspension. To understand the magnitude and timing of resuspension, a comparison of calculated maximum horizontal bed velocities from a long-term wave and current hindcast model with resuspension thresholds from the literature was performed.

2 | Methods

2.1 | Study Site

Herschel Island–Qikiqtaruk (HIQ) is located about 3 km offshore in the southern Canadian Beaufort Sea in the Yukon, Canada (Figure 1). The island is about 116 km^2 in size and geographically separated from the mainland by the Workboat Passage, a shallow depositional area, which is bordered by multiple dynamic sediment spit systems [4, 21]. Eastward of the island lies a depression called Herschel Basin. The basin is a remnant of the excavation by an advancing side lobe of the Laurentide Ice Sheet during the later phase of the Wisconsin glaciation, excavating and pushing up the marine and terrestrial sediments that form the HIQ endmoraine [26, 27]. The up to 180-m-high island is characterized by ice-rich permafrost sediments of glacial origin overlain by a layer of Holocene peat and organic material [21].

The western Canadian Beaufort Sea is influenced by the discharge of relatively warm water from the Mackenzie River, which is the 4th largest river system in the Arctic by discharge (about 325 km^3/year) and delivers the highest amount of sediment among the big Arctic rivers [28, 29]. Riverine water and sediment dispersal in the Beaufort Sea starts around the end of May, whereas the exact distribution of the water depends on regional wind conditions and the location of sea ice [30]. Mackenzie River water has a temperature of up to 15°C and can extend over large parts of the southern Canadian Beaufort Sea and even westward beyond HIQ, which is about 120 km away from the river mouth [30, 31].

The ice breakup around HIQ usually occurs around mid-May, whereas due to the bottom topography at Herschel Sill, sea ice freezes to the bottom (bottom-fast ice) and is attached to the coast (landfast ice) so that it forms a solid ice cover that delays the complete opening of the island's coast until mid-June. This results in an effective open water period of about 4 months until mid-October. During that period, the length of the fetch (length of water over which the wind can blow) is often 100 km or longer, as indicated by Canadian Ice Service charts. Sea ice may retreat up to 500 km offshore in summer in

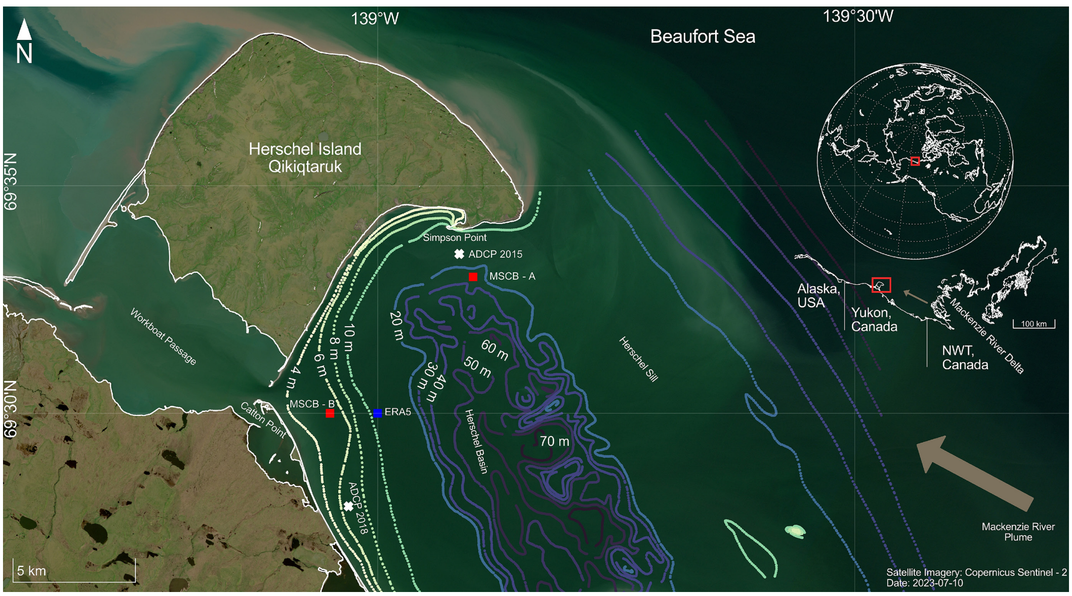

FIGURE 1 | Study area of Herschel Island–Qikiqtaruk in the western Canadian Arctic. The background image is a true color Sentinel-2 satellite image from July 10, 2023, showing typical summer season sediment plumes along the coastal areas in mainly sea-ice free waters. The squares indicate the location of the MSC Beaufort (MSCB) wave and current hindcast (red) and the ERA5 atmospheric reanalysis grid point (blue). White crosses show the study sites, that is, the Acoustic Doppler Current Profiler (ADCP) mooring positions and the year of deployment. Bathymetry is taken from O'Connor [24], showing the 4-, 6-, 8-, 10-, 20-, 30-, 40-, 50-, 60-, and 70-m isobaths. Bathymetry colormap based on Thyng et al. [25]. [Colour figure can be viewed at wileyonlinelibrary.com]

the Canadian Beaufort Sea [32, 33]. The coast around HIQ is microtidal with a mixed-semidiurnal pattern with tidal ranges from 0.15 to 0.25 m [34].

Around HIQ, storms and strong winds are observed in a bimodal pattern, with the major storm component from the northwest and a minor component from the southeast (Appendix S1, [35]). This leads to more developed waves along the northwest facing coasts, in comparison to coasts facing towards the southeast [36]. In the Beaufort Sea, storm waves are believed to be the main driver for coastal sediment transport [37, 38]. The decadal regional average erosion rate along the mainland coast of the Yukon is 1.3 m/year with spatial differences [4]. HIQ has a reported erosion rate of 0.68 m/year (2000–2011) [22]. Shoreline changes are taking place all over the island and occur through retrogressive thaw slumps, active layer detachments, and bluff erosion. Spit systems around HIQ are migrating with net movement in longshore and onshore direction controlled by storm waves and sediment supply [37, 39, 40].

2.2 | Meteo-Oceanographic Data Acquisition

2.2.1 | ERA5 Wind Reanalysis

The ECMWF Reanalysis v5 (ERA5) wind reanalysis was used to provide wind hindcast. The ERA5 reanalysis provided hourly wind direction and wind speed for this study [41, 42], because the wind record from the closest WMO meteorological station of HIQ showed too many gaps. The ERA5 product spans from January 1940 to present day, providing hourly data along a global spatial grid of 0.25° (31 km). Recent studies in the Beaufort Sea region found a good agreement between ERA5 and the HIQ weather station recording, even though the data from the weather station was not assimilated into the ERA5 reanalysis product [31, 43]. The model grid point at N69.5°, W139° (blue square on Figure 1) was less than 10 km away from the mooring locations and was used here for wind data. ERA5 data were loaded into tables to calculate mean and extreme values for the study period and 30-year averages of wind speed for each month (June to October) in the open-water season. The term "storm" is used after the definition for Arctic coasts that storms are events of wind speed exceeding > 10 m/s for more than 6 h [44]. Data analysis was performed using MATLAB 2023b for this and all other used datasets in this study [45, 46].

2.2.2 | MSCB Wave and Current Reanalysis

The MSC50 Wind and Wave Climate Hindcast [47, 48] was used to provide a continuous wave hindcast. This wave hindcast product provides hourly oceanographic data, and information about sea ice is updated weekly into the model [49]. The hindcast domain for the Beaufort Sea extends along a grid of about 6×6 km covering the Canadian Beaufort Sea from N69.45° to N72.00° and W126.00° to W142.50°. The MSCB extends temporally from January 1970 to December 2018. Due to the high spatial and temporal resolution and the frequently updated regional sea ice position, the MSCB was used successfully in previous studies in the Beaufort Sea [49–51]. Recently, current velocity and direction produced with the ADCIRC (*An Advanced Three-Dimensional Circulation Model for Shelves, Coasts, and Estuaries*) model were included in the output, but not in the production of the model [52, 53]. The ADCIRC hydrodynamic model was forced with astronomic tides, wind stress, and atmospheric pressure data adapted to ice conditions [54]. The data outputs are given as vertically averaged hourly values of current velocity and direction for the MSCB temporal and spatial domain. The MSCB output point "217" (bathymetry of 20.5 m) is hereafter named Point A and is the closest point to the field study site in 2015. The MSCB output point "183" (bathymetry of 5 m) is hereafter named Point B and is the closest point to the field study site in 2018 (see Figure 1).

The 49-year-long MSCB data set was used to calculate average and maximum significant wave height and current velocity values for the study period and to relate these values to the seasonal and long-term data. The data set was also used to calculate the maximum horizontal velocity at bed, which is often used to indicate if sediment can get resuspended [55]. It was calculated using Hs (significant wave height), Tp (peak period), and h (water depth) values from the MSCB for both study sites (red squares in Figure 1). The simplified expression formula from Davidson-Arnott et al. [55] was implemented in MATLAB; the results are presented in Figure 2.

2.2.3 | In Situ ADCP Measurements

In 2015 and 2018, a custom-made stainless steel mooring platform containing a 600-kHz Teledyne Workhorse Sentinel ADCP was deployed in the nearshore zone close to the Herschel Basin (N69.5584°, W138.9144° and N69.4658°, W139.0306°; Figure 1). An ADCP is an underwater device that uses passively drifting particles in the water column to derive current velocity and direction by sending ultrasonic sound waves and receiving their echo. At both study sites, the ADCP was used as a stationary instrument to measure the water flow in bins from the sea bottom to the sea surface. In 2015, the ADCP was measured current velocity and direction at a 15-min interval. The sensor was placed in 12 m depth, 1 km offshore, and was retrieved after 17 days. In 2018, the ADCP was measured every minute for 14 days. It was placed about 1 km offshore, at 7 m water depth. The size of the bins was set to 0.5 m; the first bin covered 1.6 to 2.1 m above the seafloor. The uppermost bin in 2015 covered 10.1 to 10.6 m and in 2018 covered 4.6 to 5.1 m above the seafloor; bins above this are disregarded due to air bubbles, echo interference, and turbulences [56–59]. The detailed deployment procedure for the ADCP moorings and the data preprocessing is described in two data publications [60, 61].

The ADCP-based current measurements (eastward and northward component of the flow) were averaged to hourly values. Measured current velocities and directions were visualized using an adaptation of the "provec" function from the jLab oceanographic function toolbox [62]. This allowed a better visualization of differences in potential transport directions between the upper and lower water column at the study sites. To relate the measured bottom currents to sediment transport and sediment resuspension, critical bottom shear-velocity values from the Canadian Beaufort shelf of 10–40 cm/s [63] and 18–36 cm/s [64] are used to compare the velocity data to the characteristics of bottom sediment in the nearshore zone around HIQ.

2.2.4 | Grain Size Analysis

Nearshore sea floor surface sediments were collected in 2016 with a gravity corer (15 short cores), in 2018 with one Van-Veen grab sample and in 2019 with gravity coring (two cores). Sampling followed two transects A and B from the coast to the basin (see Figure 5, [11]). The upper 0–2 cm of sediment from the gravity cores were subsampled for grain-size analyses, and the results were averaged. Sediment samples were treated according to a standard protocol with H_2O_2 to remove organic material [65]. The grain size distributions were obtained using a laser diffractometry analyzer (Malvern Mastersizer 3000, Malvern Panalytical, United Kingdom). Sorting was calculated with the graphical method [66, 67], and the mean grain size was calculated and named based on the standardized size scale [66]. The number of measurements was enhanced with 205 existing sediment data points from regional Van-Veen surface samples using the mean grain size and sorting method based on (Folk & Ward method, Graphic micron fraction < 1 mm) [35, 40].

3 | Results

3.1 | ERA5 Wind Data

The 30-year (1991–2020) mean wind speed at HIQ was 4.29 m/s (June to October), with a maximum wind speed of 16.17 m/s on September 1, 2015. Overall wind speed distribution showed a seasonal trend with 4.09 m/s in June, 4.14 m/s in July, 4.30 m/s in August, 4.55 m/s in September, and 4.37 m/s in October. The wind direction was bimodal: (1) The main wind direction was WNW-NW with on average 44.2 h of wind speeds above the 10 m/s threshold for Arctic storms per year (June to October) [44]. (2) The secondary wind direction was SE-SES with on average only 4.1 h of wind speeds above 10 m/s per year (Jun-Oct) (Appendix S1, upper plot).

For the observation period in 2015, the mean recorded wind speed was 4.33 m/s. The distribution of winds during this period was similar to the observed bimodal distribution (Appendix S1, middle plot). The maximum recorded value for this period was 11.73 m/s (WNW) on August 11 at (03:00) (all datetimes in this study are in UTC-6 h); this is the only classified storm event and lasted for 16 h. For the mooring period in 2018, the mean recorded wind speed was 4.91 m/s, which is slightly above the long-term mean. The maximum recorded value for this period was 12.04 m/s (WNW) on August 17 at (06:00) in an 8-h-long storm event. The period compares to the observed wind strength during the other mooring period in 2015 (Appendix S1, lower plot).

3.2 | MSCB Waves and Currents

The hydrodynamical record in the open water season (June to October) is obtained from the MSCB wave and current model providing output for two points close to the current measurement

TABLE 1 | Monthly statistics (1970 to 2018) of wave height, current speed, and maximum horizontal bed velocity from the MSCB for the two study sites.

Site	Month	Mean significant wave height (m)	Mean current speed (cm/s)	Median maximum horizontal bed velocity (cm/s)	Highest maximum horizontal bed velocity (cm/s)
A	Jun	0.37	4.8	0	17.7
A	Jul	0.3	5.8	0	20
A	Aug	0.37	8.7	0.1	46.7
A	Sep	0.65	12.5	0.8	67.5
A	Oct	0.87	11.4	1.6	87.5
B	Jun	0.23	3.6	1.3	59.8
B	Jul	0.19	5	1.8	56.1
B	Aug	0.24	7.6	4.7	98.2
B	Sep	0.42	11.4	14.3	123
B	Oct	0.54	9.6	19.3	136.7

sites (Figure 1). In Table 1, the 48-year (1970–2018) data set of mean significant wave height and current speed is grouped by months.

The data for the two study sites show calm wave conditions of 0.19 to 0.37 m of mean significant wave height for the months of June, July, and August. During September and October, wave heights increased at Study Site A (B) to 0.65 (0.42) m and 0.87 (0.54) m.

The mean current speeds varied through the season with a minimum in June at both sites 4.8 (A) and 5.0 cm/s (B) and a maximum of 12.5 (11.4) cm/s in September. The median maximum horizontal bed velocity is below 2 cm/s during the whole season at Site A, and during June and July at Site B with an increase in August, September and October to 4.7, 14.3, and 19.3 cm/s. The highest maximum horizontal bed velocity gradually increases at both sites from record 17.7 cm/s in June towards 87.5 cm/s in October at Site A and 59.8 cm/s in June and 136.7 cm/s in October at Site B. These large differences between the study sites likely reflect the different depths of both analysis points.

The 48-year long MSCB record provides the opportunity to observe long-term trends in hydrodynamics (Figure 2). The current speed shows a moderate variability with a mean of 8.6 ± 4.3 cm/s at Site A and 7.5 ± 3.8 cm/s at Site B without any trend. The yearly number of open water days, calculated as the aggregated hours of significant wave heights above 0 cm per year, is more variable. Between 1970 and 2000, the length was about 90 days (56 and 133 in extreme years) for both study sites. Since the year 2010, 130 days are the norm, with 2012 and 2016 as extreme years of 161 and 168 open water days at Site A, elongating the open water period by more than 1 month.

The maximum horizontal bed velocities differ significantly at both sites. Although the median and maximum values are not directly following the minima of sea-ice extent, they often respond to it. For Site A (respectively B), the highest recorded velocity was for years with low sea ice (2006, respectively 1998), but these years were not record low sea ice years, highlighting the role of other factors, potentially strong storms, in driving current velocity. However, the 75th percentile of the maximum horizontal bed velocity values rises in line with the length of the open water period over the last decades.

During the in situ measurements from July 28, 2015 (0:00), to August 13, 2015 (15:00), the mean significant wave height was 0.31 m with a maximum of 0.99 m on August 8, 2015 (2:00). The mean vertically averaged current velocity was 7.3 cm/s, with a recorded maximum of 23.0 cm/s on August 2, 2015 (00:00). During the second ADCP measurement period (August 4, 2018 [01:00], to August 18, 2018 [13:00]), the mean significant wave height was 0.28 m with a maximum of 0.82 m on August 5 at 04:00. The mean vertically averaged current velocity was 9.4 cm/s, with a recorded maximum of 39.2 cm/s on August 5 at 18:00 (Figure 3).

3.3 | ADCP Current Measurements

The ADCP was deployed from July 28, 2015 (0:00), to August 13, 2015 (15:00), at Study Site A and from August 4, 2018 (01:00), to August 18, 2018 (13:00), at Study Site B (for locations, see Figure 1).

At Study Site A in 2015, the recorded mean current velocity close to the sea bottom was 9.1 cm/s, with a maximum value of 31.8 cm/s on August 9 at 10:00 (Figure 3). The flow direction showed a bimodal pattern with an onshore (NNW-N) and offshore (SSE-SE) directed flow, perpendicular to the shoreline. The potential cumulative net drift (see Figure 4, upper red line) was 14.4 km offshore but was characterized by a frequent change in direction along the onshore-offshore direction.

At the surface, the average flow velocity was 17.9 cm/s, with a maximum current velocity of 61.8 cm/s on August 10 at 04:00. The flow velocity was inconsistent, but without a visible periodicity during the measurements. The potential cumulative net drift (see Figure 4, upper blue line) was 157.9 km offshore

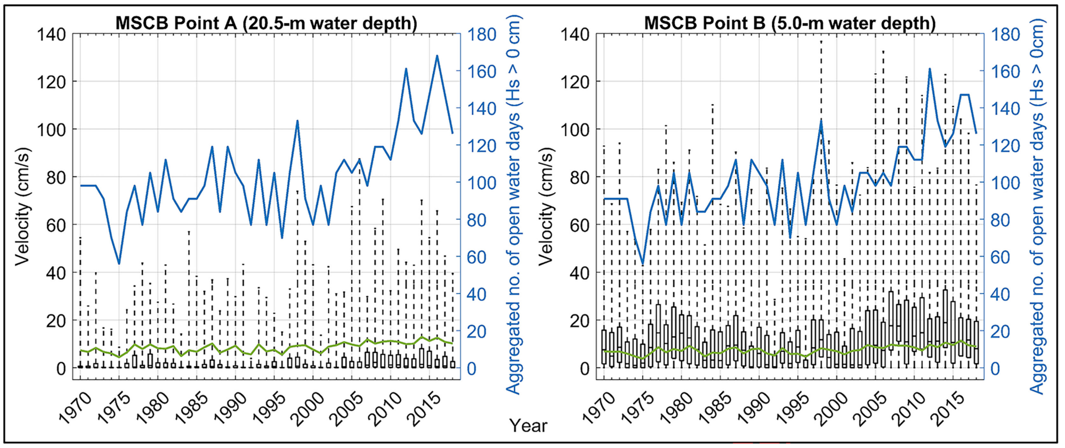

FIGURE 2 | Time series of current and bed velocities coupled to the length of the open water season for MSCB Points A and B. Left axes show the MSCB-derived current (green line) and the maximum horizontal bed (boxplot) velocity statistics from 1970 to 2018 (June to October). Right axes show the annual number of open water days from 1970 to 2018 (blue line) derived from the annual hours of significant wave height (H_s) above 0 cm. Boxplots: center line—median value, box: 25th and 75th percentile of the data, black range (min to max) of the data. [Colour figure can be viewed at wileyonlinelibrary.com]

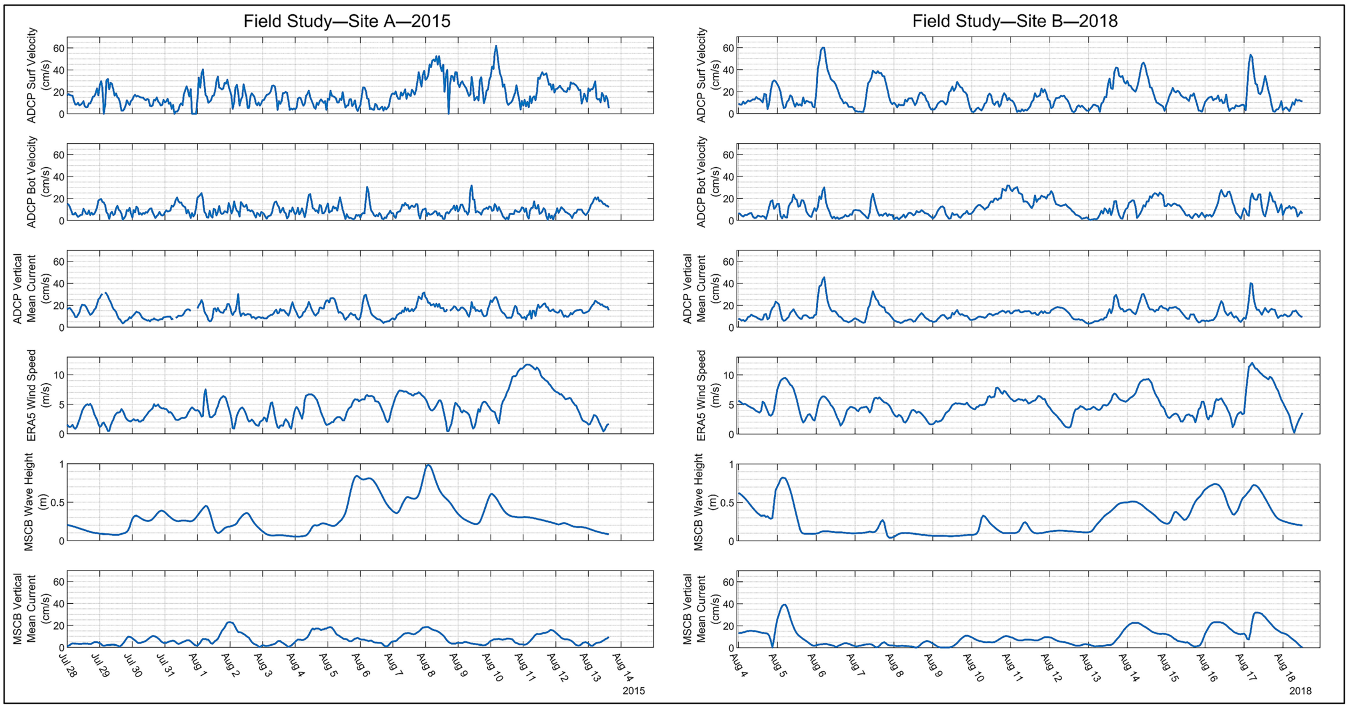

FIGURE 3 | Time series of ADCP measurements surface (surf), bottom (bot), vertically averaged, and reanalysis data (ERA5 wind speed, MSCB significant wave height, and vertically averaged current velocity) at Study Sites A and B. For Study Site A, the data cover the period from July 28 to August 13, 2015. For Study Site B, the data cover the period from August 4 to August 18, 2018. Parameters from top to bottom: ADCP surface column velocity in cm/s, ADCP bottom column velocity in cm/s, vertically averaged ADCP velocity in cm/s, ERA5 wind speed in m/s, MSCB significant wave height in m, and MSCB vertically averaged current velocity in cm/s. [Colour figure can be viewed at wileyonlinelibrary.com]

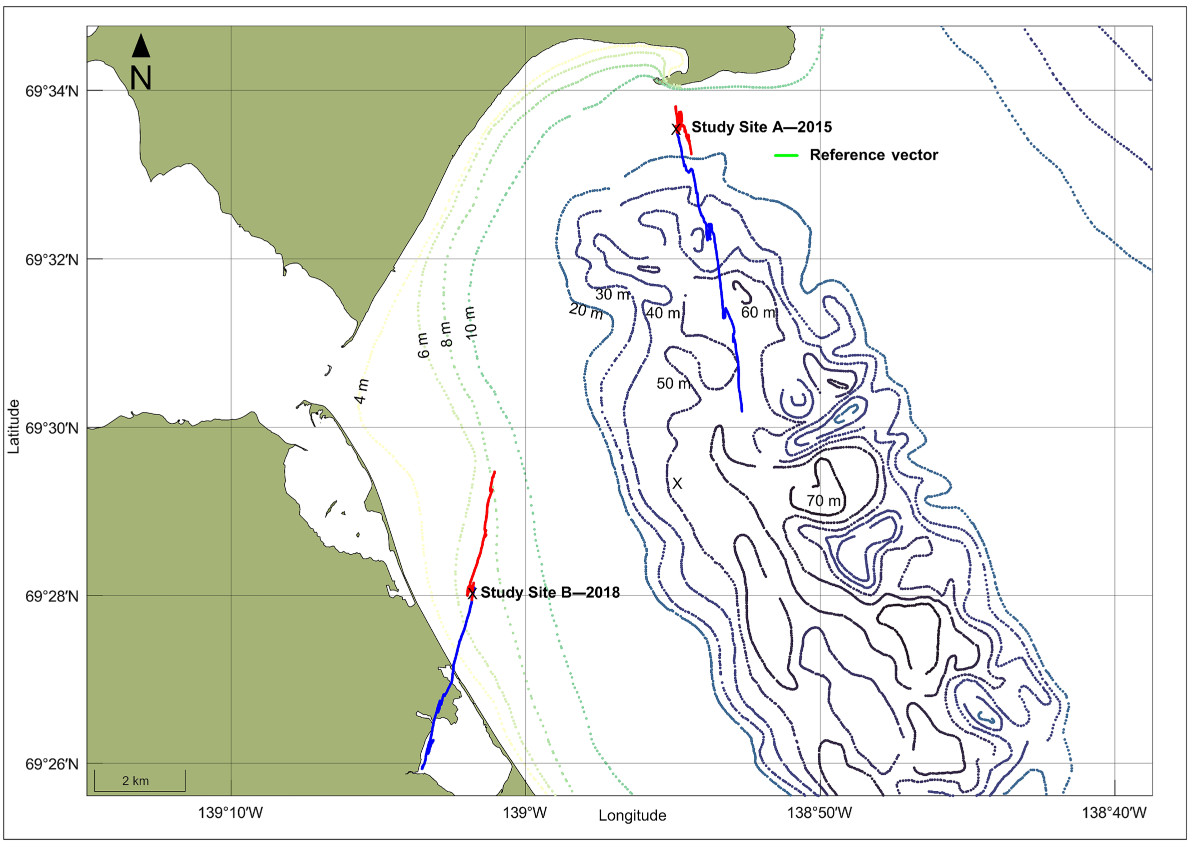

FIGURE 4 | ADCP measurements plotted as *cumvec*-plot transferring stationary measurements into a potential cumulative net drift [62]. Applied scaling is 1 to 25, to fit the distances on the map, small green line as a scaling reference (1 day of constant eastward flow of 20 cm/s). Surface flow in blue color. Bottom flow in red color. Note the different years and lengths of the measurements. [Colour figure can be viewed at wileyonlinelibrary.com]

(towards SSE), spanning a much larger distance than the one calculated for the bottom currents. Changes to the overall flow direction occurred, but to a much smaller magnitude than for the bottom currents. Averaged through the whole water column, the mean value was 14.6 cm/s with a maximum of 31.7 cm/s on July 29 at 04:00.

At Study Site B in 2018, the mean recorded current velocity was 11.0 cm/s at the sea bottom, with a maximum flow of 31.6 cm/s recorded on August 10 at 23:00. The potential cumulative net drift (see Figure 4, lower red line) was 71.6 km towards NNE, oblique to the shoreline towards the basin. For a short time, the flow was exactly opposite (SSW-SW) to the overall direction. At the surface, the mean recorded surface flow velocity was 15.2 cm/s, with a maximum value of 60.0 cm/s recorded on August 6 at 05:00. The potential cumulative net drift (see Figure 4, lower blue line) was 97.3 km towards SSW, although for short time periods, the drift direction was towards the opposite direction. Averaged through the whole water column, the mean value was 12.6 cm/s with a maximum value of 52.4 cm/s on August 6 at 06:00.

3.4 | Sediment Distribution

The mean grain size varied from very fine sand (64.3 μm) to fine silt (5.4 μm). At depths greater than 12 m, the sediment was made of fine to medium silt (data available in Appendix S2). The sediments along Transect A, located close to the 2015 ADCP measurements, were primarily silts. This contrasts with the observations made by Radosavljevic et al. [40], who found fine silts in the sheltered embayment behind Simpson Point but sediments as large as medium sand around the Simpson Point spit close to this transect (Figure 5, left inset, [40]). Overall, a strong gradient in the sediments from sands (close to the shore) towards medium silts in 8 m water depth was seen (Figure 5, left inset, gray circles, [35]). At Transect B from Catton Point towards Herschel Basin, grain sizes varied from very fine sand to fine silt. A strong change from very fine sand to medium silt was observed at the 12-m isobath. The sorting of the samples from both transects was poor to very poor (2.25 to 4.32) with slightly better sorted sediments found inside the deeper parts of the basin. Overall, it compares to the sorting previously found by Radosavljevic et al. [40] (Figure 5, right inset; Appendix S2).

4 | Discussion

4.1 | Nearshore Coastal Currents

The current velocities measured by the ADCPs showed a strong gradient between the surface and the bottom of the water column. The currents were generally greater close to the surface (average of 32 cm/s in 2015 and 2018) than at the bottom (average of 9 and 11 cm/s in 2015, 2018). The highest surface current velocities of 62 cm/s (2015) and 60 cm/s (2018) were both recorded in short events and were followed by a rapid decline. In 2018, the increase in surface current velocity was directly linked to the occurrence of higher wind speeds, albeit with a time lag. During the field study, the lag between a strong wind event and a response in the surface current had a variable duration between 1 and 23 h, resulting in no measurable correlation. Fissel and Birch [63] examined the time lag between wind and currents events for multiple recordings in the Beaufort Sea and found time-lags of up to 7 h (< 20 m water depth), with longer time-lags further offshore. The observed currents generally reflect the episodic nature of the pronounced strong wind events, where intense periods follow certain lulls in the overall variable wind conditions. In 2015, the link between winds and surface current velocities was not

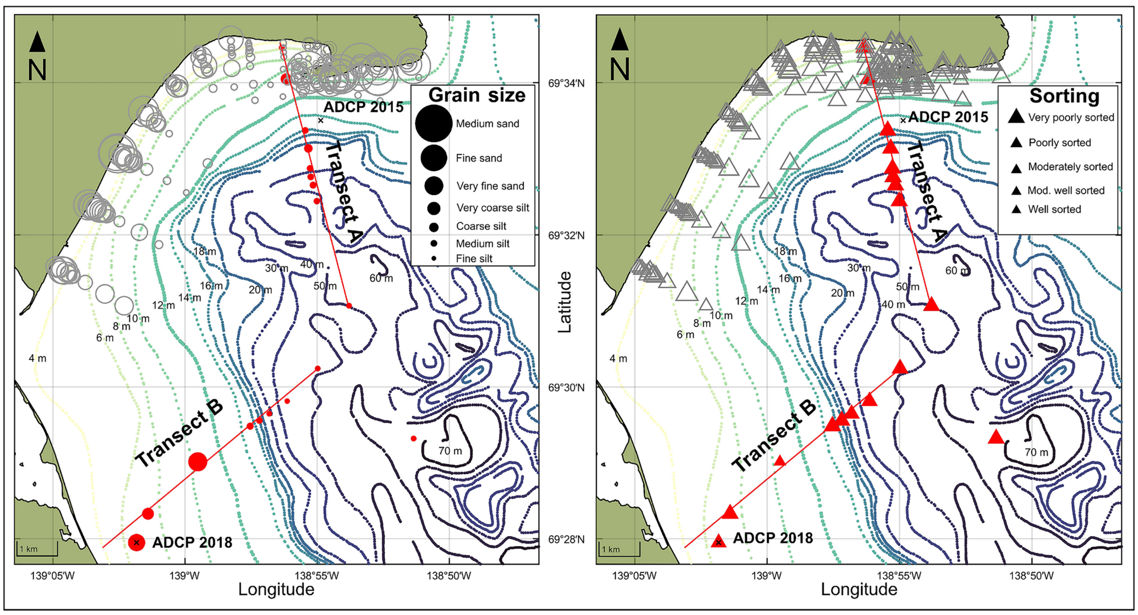

FIGURE 5 | Left, mean grain size [66]. Right, sediment sorting [67]. Central view on the Herschel Basin; see Figure 1 for location names. Gray data markers from previous measurements [35, 40]; red data markers from this study. Red lines show gravity coring locations along the two transects: A and B [11]. [Colour figure can be viewed at wileyonlinelibrary.com]

as obvious. This is particularly true for August 11, 2015. The storm recorded on that day did not lead to a substantial rise in the current velocity.

Multiple studies in the Arctic have reported that wind is the main driving force for nearshore currents: Low winds lead to drastically reduced current velocities, and storm events lead to the strongest current events [13, 20, 63, 68, 69]. Fissel and Birch [63] found that in the Beaufort Sea, the major frequency band of changes in currents happens at a synoptic period of 2 to 20 days, corresponding to the passage of regional wind systems, whereas the tidal influence is minor [20, 68, 70]. However, multiple wind-driven phenomena alter the direct response due to surges, pressure differences, and subsequent water-level differences and waves [20, 37, 68]. In our measurements, the coupling of the bottom currents to the wind (ratio between mean bottom current and wind speed) was 0.021 (2015) and 0.022 (2018), which is close to the reported value of 0.02 for West Atkinson, NWT, Canada, in 8 m water depth [63] and within the reported range of 0.01 to 0.025 for the inner Canadian Beaufort Shelf [13]. This confirms the coupling of bottom currents and wind during the measurements.

The average recorded bottom velocities of 9 cm/s (2015) and 11 cm/s (2018) are comparable to the average values of 8 to 16 cm/s for the inner shelf and the nearshore (< 20 m) zone of the Canadian Beaufort Sea [63]. The episodic nature of the current velocity, where low values of less than 20 cm/s are recorded for multiple days during calm wind conditions, was also observed by Héquette and Hill [20], where fair weather periods led to current velocities of less than 8 cm/s.

The maximum recorded near bottom current velocities of 32 cm/s (2015) and 32 cm/s (2018) are low compared to previous measurements of 40–56 cm/s (Fissel and Birch, [63]; 50 cm/s of Héquette and Hill [20]; 100 cm/s Hill et al. [13]; and 100 cm/s Weingartner et al. [68]), likely reflecting the absence of extensive strong storms during our measurements in summer, where only one moderate storm event during each measurement period was observed. This limits the applicability of our results to the relatively calm summer season.

The bottom currents tended to be lower than the surface ones, except for the period between August 10 to August 13, 2018, when bottom currents were faster. This period corresponded to the presence of open pack ice over the Herschel Basin, with mobile scattered ice floes covering locally up to 70% of the usually ice-free waters of the Southern Beaufort Sea [32]. This drastically limited the fetch length at the field sites (Figure 1) and therefore reduced surface flow velocities at that time. The simultaneous increase in bottom flow velocity could be the result of ice keel induced momentum flux, as reported by other studies under medium sea ice concentrations [43, 71, 72].

The lack of a strong relationship between the wind and the currents, especially in 2015, is likely the result of the concomitance of multiple small-scale (complex bathymetry, sheltered mooring position) and large-scale (water level surges due to pressure gradients, influence of shelf flow patterns, position of the sea ice) processes [20, 63]. The relationship is further complicated by the variability in the response time-lag based on preconditions and the wind direction. Additionally, the forcing needs to overcome the inertia of the system, and this threshold is also subject to the steadiness of the wind direction and incoming wind intensity [20]. This is important because the angle between incident wind direction and coastal orientation results in different current responses [20, 63]. In the Beaufort Sea, water column stratification due to the pronounced Mackenzie River plume, as well as upwelling and downwelling events, is also adding complexity to the linkage between wind forcing and current velocity response [68, 73, 74].

The currents observed in 2015 and 2018 were primarily perpendicular or oblique to the shoreline. In 2015, the net direction of bottom and surface flows was directed offshore towards Herschel Basin with an occasional reversal of the flow. In 2018, the net flows at the bottom and the surface layer were in opposite directions, albeit in a general axis oblique to the shorelines. This contrasts with findings from other authors along most stretches of the Beaufort Sea coast, where a pronounced along-shore coastal current flowed parallel to the local bathymetry [63, 68]. West of HIQ, Lin et al. [43] observed a pronounced longshore coastal flow. Local effects linked to the sheltering effect of the island of HIQ and the presence of mobile sea ice likely led to the reduction of the along-shore current potential [13]. The Mackenzie River plume front was previously connected to perpendicular or slightly oblique to the shoreline directed flow directions [13, 20, 63]. Although it could have influenced the currents for a period, it is rather unlikely the plume front constantly affected the measurements.

The vertically averaged MSCB current velocities are slower compared to the measured currents in both study periods. Although the model generally captures the frequency and magnitude of the pronounced current events, it does not resolve the moderate events in great detail. The timing of the modeled high velocity events retrieved from the MSCB reanalysis differed from the recorded measurements by up to 1 day. This time lag was particularly prominent on August 6, 2018, when the strongest currents were measured.

4.2 | Sediment Transport

Much of the organic-rich permafrost material eroded at the coast is released to the nearshore zone. There, it is likely to undergo a series of processes leading to transport, degradation, and deposition [8, 10, 75]. Traditionally, authors have considered that the eroded material was transported offshore and deposited there, yet a growing number of studies show that coastal resuspension may play an important role in sediment transport and organic matter degradation [9, 16]. Our bottom current velocity measurements were all below or close to the lower boundary of this range, indicating that no lasting sediment resuspension would have taken place. This is hardly surprising because our sampling periods were characterized by moderate winds, and sediment resuspension is more likely to occur during autumn storms.

It was observed, however, that in these wind conditions, resuspension can occur in shallower water depths, along a gradient from the shore to the sea [12]. This gradient was also observed by Klein et al. [14], who showed the continuous presence of a highly turbid fringe along the shoreline of HIQ in Landsat imagery collected over a 30-year period. Our sampling locations at Points A and B were not located in the immediate vicinity to the shoreline and could not capture resuspension very close to the shore.

The maximum horizontal bed velocities from the MSCB showed that in 20 m depth (at the edge of the nearshore zone), resuspension would be limited to prominent October storms [13], whereas at 5 m water depth, resuspension would frequently take place during September and October, with occasional events in August [20, 76]. This shows that the potential for resuspension greatly increases in shallow waters and is linked to seasonality.

This resuspension potential gradient is reflected in the grain size from the two sea floor transects. On exposed shorelines, the grain size decreased drastically from the shoreline to the offshore. Jong et al. [12] showed that deposition occurred only beyond a critical depth. Our data show that beyond 12 m depth, the small fraction (fine to medium silts) dominated. Fine grained sediments were also found close to the shoreline, albeit in a sheltered low-energy nearshore deposition center behind Simpson Point [35].

Sediment mobilization potential in the nearshore zone is therefore primarily related to wind forcing but can be strongly diminished by the presence of sea ice. During open-water storm events, sediments up to fine sand are mobilized in the water column [13, 20, 77]. Fissel and Birch [63] observed in the Beaufort Sea that greater turbidity at depth was associated with greater waves. This was also supported by findings of sediment-covered instruments in the nearshore zone [68]. These observations have strong implications for the future state of the Arctic nearshore zone, because larger fetches, longer open water season, and decreased sea ice extent could enhance sediment mobilization and dispersal.

4.3 | Implications

Arctic warming leads to the shrinkage of the seasonal sea ice coverage, to the lengthening of the open-water season and to an increase in wave heights [6]. The general increase in wave forcing would potentially lead to greater transport of eroded material. Sediment resuspension is also largely driven by wave forcing. From the year 2000 onwards, a rise in the average horizontal bed velocities in line with the elongating open water period is visible. Although an interseasonal variability remains, less ice coverage increases the potential for more sediment mobilization in the Beaufort Sea region. A larger fetch during the stormy season would lead to more reworking of the sediments. Sediment transport could be greater during months already characterized by open water conditions (July, August, and September) and during months previously dominated by sea ice presence (October and November).

In the Canadian Beaufort Sea, the dominant incident wave direction was historically from the northwest. Recent studies have noted a shift towards more eastern conditions, which would increase the frequency of larger wave events into regions around the Herschel Basin, which are otherwise sheltered from northwest storms [36, 49, 78]. The enhanced turbidity linked to resuspension could potentially lead to substantial changes to the coastal biogeochemical budget through an added increase in carbon and nutrients. It already has direct impacts on the microfauna in the nearshore zone [78] and potentially alters sedimentary-bound carbon transport [12, 16].

5 | Conclusion

In situ measurements of coastal currents along permafrost coasts are challenging. The presence of sea ice prevents the use of techniques used at lower latitudes. Arctic nearshore currents are therefore poorly understood, and data are scarce. Yet nearshore currents play a crucial role in mobilizing eroded coastal permafrost material and determine the fate of sediments and organic matter in the nearshore zone.

This study reported on current measurements using ADCPs deployed in 7 and 12 m depths for a short season in the vicinity of Herschel Island–Qikiqtaruk, Yukon, Canada. At both locations, the current velocity was stronger in the upper than in the lower water column. The potential drift direction showed that currents in the lower water column pointed in a net offshore direction. The surface water currents were directed either offshore (2015) or in an oblique onshore direction (2018). These contrasting pathways in the lower water column are due to multiple factors acting upon the small and large synoptic scales.

The current velocity was mainly driven by the intensity of the wind. The current velocity increased drastically during a storm event in 2018 but did not in 2015, where no clear current velocity response could be detected during strong wind events. Previous studies linked this variable response to differences in the wind direction, sea ice coverage, the pronounced water stratification from the Mackenzie River plume, and large-scale circulation systems. Our results suggest that coastal promontories such as HIQ play an important role in controlling the relationship between wind and currents. The comparison of in situ ADCP current measurements with the MSCB reanalysis data shows that both datasets generally agree but that some substantial discrepancies remain. The modeled events often lagged behind the measured ones by up to a day. Short events were often missed by the model, whereas longer and more intense events were adequately captured. Overall, the measured currents were often faster than the modeled ones.

This study opens opportunities to investigate coastal currents along permafrost coasts, where the deployment of instruments is often costly and challenging. Yet our in situ measurements covered very limited time spans, and future efforts should be focusing on the acquisition of comprehensive wave and current datasets over the entire open-water season. This would help validate reanalysis datasets and to provide the boundary conditions required to develop accurate models of coastal hydrodynamics. This is crucial to the compilation of coastal sediment and biogeochemical budgets and the projection of the impact of coastal erosion along permafrost coasts.

Acknowledgments

The authors are very grateful to the Government of Yukon and Yukon Parks for permitting this research. We thank the rangers of Herschel Island–Qikiqtaruk Territorial Park, as well as George Tanski, Niek J. Speetjens, Samuel Stettner, Anna M. Irrgang, Boris Radosavljevic, and Jade Falardeau for their help during fieldwork. We want to acknowledge the Aurora Research Institute (ARI, Inuvik) for logistical support and the AWI sedimentary lab staff. We also want to thank Arnaud Héquette and Frederieke Miesner for their fruitful thoughts on the data and data processing. This project has received funding from the European Union's Horizon 2020 research and innovation programme under Grant Agreement No. 773421.

Conflicts of Interest

The authors declare no conflicts of interest.

Data Availability Statement

The ADCP data used in this study can be accessed at the open access data repository PANGAEA (https://doi.pangaea.de/10.1594/PANGAEA.931908 and https://doi.pangaea.de/10.1594/PANGAEA.931914) [60, 61]. MATLAB scripts to process the data and recreate the figures are available in a GitHub repository (under https://github.com/jgimsa/Gimsa-2024-Data).

References

1. H. Lantuit, P. P. Overduin, N. Couture, et al., "The Arctic Coastal Dynamics Database: A New Classification Scheme and Statistics on Arctic Permafrost Coastlines," *Estuaries and Coasts* 35 (2012): 383–400.

2. F. E. Aré, "Thermal Abrasion of sea Coasts (Part I)," *Polar Geography and Geology* 12 (1988): 1, https://doi.org/10.1080/10889378809377343.

3. F. Günther, P. P. Overduin, I. A. Yakshina, T. Opel, A. V. Baranskaya, and M. N. Grigoriev, "Observing Muostakh Disappear: Permafrost Thaw Subsidence and Erosion of a Ground-Ice-Rich Island in Response to Arctic Summer Warming and Sea Ice Reduction," *Cryosphere* 9, no. 1 (2015): 151–178.

4. A. M. Irrgang, H. Lantuit, G. K. Manson, F. Günther, G. Grosse, and P. P. Overduin, "Variability in Rates of Coastal Change Along the Yukon Coast, 1951 to 2015," *Journal of Geophysical Research: Earth Surface* 123, no. 4 (2018): 779–800.

5. B. M. Jones, L. M. Farquharson, C. A. Baughman, et al., "A Decade of Remotely Sensed Observations Highlight Complex Processes Linked to Coastal Permafrost Bluff Erosion in the Arctic," *Environmental Research Letters* 13, no. 11 (2018): 115001.

6. M. Casas-Prat and X. L. Wang, "Sea Ice Retreat Contributes to Projected Increases in Extreme Arctic Ocean Surface Waves," *Geophysical Research Letters* 47, no. 15 (2020): e2020GL088100.

7. D. M. Nielsen, P. Pieper, A. Barkhordarian, et al., "Increase in Arctic Coastal Erosion and Its Sensitivity to Warming in the Twenty-First Century," *Nature Climate Change* 12, no. 3 (2022): 263–270.

8. M. Fritz, J. E. Vonk, and H. Lantuit, "Collapsing Arctic Coastlines," *Nature Climate Change* 7, no. 1 (2017): 6–7.

9. G. Tanski, D. Wagner, C. Knoblauch, M. Fritz, T. Sachs, and H. Lantuit, "Rapid CO2 Release From Eroding Permafrost in Seawater," *Geophysical Research Letters* 46, no. 20 (2019): 11244–11252.

10. G. Tanski, H. Lantuit, S. Ruttor, et al., "Transformation of Terrestrial Organic Matter Along Thermokarst-Affected Permafrost Coasts in the Arctic," *Science of the Total Environment* 581 (2017): 434–447.

11. H. Grotheer, V. Meyer, T. Riedel, et al., "Burial and Origin of Permafrost-Derived Carbon in the Nearshore Zone of the Southern Canadian Beaufort Sea," *Geophysical Research Letters* 47, no. 3 (2020): e2019GL085897.

12. D. Jong, L. Bröder, G. Tanski, et al., "Nearshore Zone Dynamics Determine Pathway of Organic Carbon From Eroding Permafrost Coasts," *Geophysical Research Letters* 47 (2020): e2020GL088561, https://doi.org/10.1029/2020GL088561.

13. P. R. Hill, S. M. Blasco, J. R. Harper, and D. B. Fissel, "Sedimentation on the Canadian Beaufort Shelf," *Continental Shelf Research* 11, no. 8–10 (1991): 821–842.

14. K. P. Klein, H. Lantuit, B. Heim, F. Fell, D. Doxaran, and A. M. Irrgang, "Long-Term High-Resolution Sediment and Sea Surface Temperature Spatial Patterns in Arctic Nearshore Waters Retrieved Using 30-Year Landsat Archive Imagery," *Remote Sensing* 11, no. 23 (2019): 2791.

15. L. Bröder, T. Tesi, J. A. Salvadó, I. P. Semiletov, O. V. Dudarev, and Ö. Gustafsson, "Fate of Terrigenous Organic Matter Across the Laptev Sea From the Mouth of the Lena River to the Deep sea of the Arctic Interior," *Biogeosciences* 13, no. 17 (2016): 5003–5019.

16. D. Jong, L. Bröder, T. Tesi, et al., "Selective Sorting and Degradation of Permafrost Organic Matter in the Nearshore Zone of Herschel Island (Yukon, Canada)," *Journal of Geophysical Research: Biogeosciences* 129 (2024): e2023JG007479, https://doi.org/10.1029/2023JG007479.

17. J. E. Vonk, I. P. Semiletov, O. V. Dudarev, et al., "Preferential Burial of Permafrost-Derived Organic Carbon in Siberian-Arctic Shelf Waters," *Journal of Geophysical Research: Oceans* 119, no. 12 (2014): 8410–8421.

18. S. M. Gay, III and S. L. Vaughan, "Seasonal Hydrography and Tidal Currents of Bays and Fjords in Prince William Sound, Alaska," *Fisheries Oceanography* 10 (2001): 159–193.

19. K. M. Stafford, S. R. Okkonen, and J. T. Clarke, "Correlation of a Strong Alaska Coastal Current With the Presence of Beluga Whales Delphinapterus Leucas Near Barrow, Alaska," *Marine Ecology Progress Series* 474 (2013): 287–297.

20. A. Héquette and P. R. Hill, "Storm-Generated Currents and Offshore Sediment Transport on a Sandy Shoreface, Tibjak Beach, Canadian Beaufort Sea," *Marine Geology* 113 (1993): 283–304.

21. J. Obu, H. Lantuit, M. Fritz, W. H. Pollard, T. Sachs, and F. Günther, "Relation Between Planimetric and Volumetric Measurements of Permafrost Coast Erosion: A Case Study From Herschel Island, Western Canadian Arctic," *Polar Research* 35, no. 1 (2016): 30313.

22. J. Obu, H. Lantuit, I. Myers-Smith, B. Heim, J. Wolter, and M. Fritz, "Effect of Terrain Characteristics on Soil Organic Carbon and Total Nitrogen Stocks in Soils of Herschel Island, Western Canadian Arctic," *Permafrost and Periglacial Processes* 28, no. 1 (2017): 92–107.

23. J. L. Ramage, A. M. Irrgang, A. Morgenstern, and H. Lantuit, "Increasing Coastal Slump Activity Impacts the Release of Sediment and Organic Carbon Into the Arctic Ocean," *Biogeosciences* 15, no. 5 (2018): 1483–1495.

24. M. Fritz, S. Wetterich, L. Schirrmeister, et al., "Eastern Beringia and Beyond: Late Wisconsinan and Holocene Landscape Dynamics Along the Yukon Coastal Plain, Canada," *Palaeogeography, Palaeoclimatology, Palaeoecology* 319 (2012): 28–45.

25. J. R. Mackay, "Glacier Ice-Thrust Features of the Yukon Coast," *Geographical Bulletin* 13, no. 5 (1959): 21.

26. M. J. O'Connor "Surficial Geology and Granular Resources Southeast of Herschel Island," (1984).

27. K. M. Thyng, C. A. Greene, R. D. Hetland, H. M. Zimmerle, and S. F. DiMarco, "True Colors of Oceanography: Guidelines for Effective and Accurate Colormap Selection," *Oceanography* 29, no. 3 (2016): 9–13.

28. V. Rachold, H. Eicken, V. V. Gordeev, et al., "Modern Terrigenous Organic Carbon Input to the Arctic Ocean," in *The Organic Carbon Cycle in the Arctic Ocean*, (Berlin, Heidelberg: Springer Berlin Heidelberg, 2004): 33–55.

29. S. B. Rood, S. Kaluthota, L. J. Philipsen, N. J. Rood, and K. P. Zanewich, "Increasing Discharge From the Mackenzie River System to the Arctic Ocean," *Hydrological Processes* 31, no. 1 (2017): 150–160.

30. T. J. Weingartner, S. L. Danielson, J. L. Kasper, and S. R. Okkonen, "Circulation and Water Property Variations in the Nearshore Alaskan Beaufort Sea (1999–2007)," Final Report U.S. Department of Interior, Minerals Management Service, Anchorage, Alaska, p. 103 OCS Study MMS 2005-028, (2009).

31. K. P. Klein, H. Lantuit, and R. J. Rolph, "Drivers of Turbidity and Its Seasonal Variability at Herschel Island Qikiqtaruk (Western Canadian Arctic)," *Water* 14, no. 11 (2022): 1751.

32. Canadian Ice Service, "CIS Archive of Daily and Weekly Ice Charts, and Daily Iceberg Charts," (2019), https://iceweb1.cis.ec.gc.ca/Archive/page1.xhtml?lang=en.

33. S. M. Solomon, "Spatial and Temporal Variability of Shoreline Change in the Beaufort-Mackenzie Region, Northwest Territories, Canada," *Geo-Marine Letters* 25, no. 2–3 (2005): 127–137.

34. Tides Canada, Tides, Currents, and Water Levels. (2023), https://tides.gc.ca/en/stations/06525.

35. B. Radosavljevic, H. Lantuit, C. Knoblauch, N. Couture, U. Herzschuh, and M. Fritz, "Arctic Nearshore Sediment Dynamics—An Example From Herschel Island—Qikiqtaruk, Canada," *Journal of Marine Science and Engineering* 10, no. 11 (2022): 1589.

36. K. Brembach, A. Pleskachevsky, and H. Lantuit, "Investigating High-Resolution Spatial Wave Patterns on the Canadian Beaufort Shelf Using Synthetic Aperture Radar Imagery at Herschel Island, Qikiqtaruk, Yukon, Canada," *Remote Sensing* 15 (2023): 4753, https://doi.org/10.3390/rs15194753.

37. A. Héquette and M. H. Ruz, "Spit and Barrier Island Migration in the Southeastern Canadian Beaufort Sea," *Journal of Coastal Research* 7, no. 3 (1991): 677–698.

38. B. M. Pinchin, R. B. Nairn, and K. L. Philpott, "Beaufort Sea Coastal Sediment Study: Numerical Estimation of Sediment Transport and Nearshore Profile Adjustment at Coastal Sites in the Canadian Beaufort Sea," *Geological Survey of Canada Open File* 1259 (1985): 712.

39. A. M. Irrgang, H. Lantuit, R. R. Gordon, A. Piskor, and G. K. Manson, "Impacts of Past and Future Coastal Changes on the Yukon Coast—Threats for Cultural Sites, Infrastructure, and Travel Routes," *Arctic Science* 5, no. 2 (2019): 107–126.

40. B. Radosavljevic, H. Lantuit, B. Plessen, and C. Knoblauch, *Granulometry and Bulk Geochemistry of Nearshore Sediments, Herschel Island, Yukon Territory, Canada* (Bremen, Germany: PANGAEA, 2016), https://doi.org/10.1594/PANGAEA.859116.

41. H. Hersbach, B. Bell, P. Berrisford, et al., "The ERA5 Global Reanalysis," *Quarterly Journal of the Royal Meteorological Society* 146, no. 730 (2020): 1999–2049.

42. H. Hersbach, B. Bell, P. Berrisford, et al., *ERA5 Hourly Data on Single Levels From 1940 to Present* (Reading, UK: Copernicus Climate Change Service (C3S) Climate Data Store (CDS), 2023), https://doi.org/10.24381/cds.adbb2d47.

43. P. Lin, R. S. Pickart, D. Fissel, et al., "Circulation in the Vicinity of Mackenzie Canyon From a Year-Long Mooring Array," *Progress in Oceanography* 187 (2020): 102396.

44. D. E. Atkinson, "Observed Storminess Patterns and Trends in the Circum-Arctic Coastal Regime," *Geo-Marine Letters* 25 (2005): 98–109.

45. MathWorks, *MATLAB 23.2 (R2023b)* (Natick, Massachusetts: MathWorks Inc., 2023), https://www.mathworks.com.

46. S. Gichuki, "Formulation of the Modulus for Wind Rose Determination," (2023), https://sgichuki.github.io/Atmo/.

47. Department of Fisheries and Ocean, "MSC50 Wind and Wave Climate Hindcast" (2023), https://meds-sdmm.dfo-mpo.gc.ca/isdm-gdsi/waves-vagues/MSC50-eng.html.

48. V. R. Swail, V. J. Cardone, B. Callahan, M. Ferguson, D. J. Gummer, and A. T. Cox, "The MSC Beaufort Wind and Wave Reanalysis," In Proc. 10th Int. Workshop on Wave Hindcasting and Forecasting and Coastal Hazard Symp (2007).

49. X. L. Wang, Y. Feng, V. R. Swail, and A. Cox, "Historical Changes in the Beaufort–Chukchi–Bering Seas Surface Winds and Waves, 1971–2013," *Journal of Climate* 28, no. 19 (2015): 7457–7469.

50. M. A. Hoque, W. Perrie, and S. M. Solomon, "Application of SWAN Model for Storm Generated Wave Simulation in the Canadian Beaufort Sea," *Journal of Ocean Engineering and Science* 5, no. 1 (2020): 19–34.

51. M. Z. Li, Y. Wu, C. G. Hannah, and W. A. Perrie, "Seabed Disturbance and Sediment Mobility due to Tidal Current and Waves on the Continental Shelves of Canada," *Canadian Journal of Earth Sciences* 58, no. 11 (2021): 1209–1232.

52. R. A. Luettich, J. J. Westerink, and N. W. Scheffner, "ADCIRC: An Advanced Three-Dimensional Circulation Model for Shelves, Coasts, and Estuaries," Report 1, Theory and methodology of ADCIRC-2DD1 and ADCIRC-3DL. (1992).

53. J. J. Westerink, R. A. Luettich, C. A. Blain, N. W. Scheffner, "ADCIRC: An Advanced Three-Dimensional Circulation Model for Shelves, Coasts, and Estuaries," Coastal Eng. Res. Cent., Vicksburg, Report, 2, (1994).

54. T. C. Massey, R. S. Chapman, M. A. Cialone, T. Hesser, R. E. Jensen, and J. M. Smith, "Including Ice Effects in a Storm Surge Modeling System". The 10th Int. Conf. on Hydroscience and Engineering (ICHE-2012), Nov. 4–Nov. 7, Orlando, USA. (2012).

55. R. Davidson-Arnott, B. Bauer, and C. Houser, *Introduction to Coastal Processes and Geomorphology* (Cambridge, UK: Cambridge university press, 2019).

56. R. L. Gordon, *Principles of Operation a Practical Primer* (San Diego: RD Instruments, 1996).

57. V. Malačič, B. Petelin, and M. Vodopivec, "Topographic Control of Wind-Driven Circulation in the Northern Adriatic," *Journal of Geophysical Research: Oceans* 117, no. C6 (2012): 1–16.

58. Teledyne RD Instruments Inc, "WorkHorse Sentinel ADCP User's Guide," (2001).

59. Teledyne RD Instruments Inc, "Workhorse Sentinel Datasheet," (2008).

60. J. Gimsa, G. Tanski, A. M. Irrgang, M. Fritz, H. Lantuit, and B. Radosavljevic, *Current Velocity Measurements From Upward-Looking ADCP at Qikiqtaruk During the Yukon Coast 2015 Expedition of the AWI* (Bremen, Germany: PANGAEA, 2021a), https://doi.org/10.1594/PANGAEA.931914.

61. J. Gimsa, G. Tanski, A. M. Irrgang, M. Fritz, and H. Lantuit, *Current Velocity Measurements From Upward-Looking ADCP at Qikiqtaruk During the Yukon Coast 2018 Expedition of the AWI* (Bremen, Germany: PANGAEA, 2021b), https://doi.org/10.1594/PANGAEA.931908.

62. J. M. Lilly, "jLab: A Data Analysis Package for Matlab, v. 1.6.6," (2019). http://www.jmlilly.net/jmlsoft.html.

63. D. B. Fissel and J. R. Birch, *Sediment Transport in the Canadian Beaufort Sea* (Dartmouth, Nova Scotia: Report by Arctic Sciences Ltd, Victoria, British Columbia for Geological Survey of Canada, 1984): 165, https://doi.org/10.4095/328851.

64. A. Forest, P. D. Osborne, G. Curtiss, and M. G. Lowings, "Current Surges and Seabed Erosion Near the Shelf Break in the Canadian

Beaufort sea: A Response to Wind and ice Motion Stress," *Journal of Marine Systems* 160 (2016): 1–16.

65. L. Schirrmeister, E. Dietze, H. Matthes, et al., "The Genesis of Yedoma Ice Complex Permafrost–Grain-Size Endmember Modeling Analysis From Siberia and Alaska," *E&G Quaternary Science Journal* 69, no. 1 (2020): 33–53.

66. S. J. Blott and K. Pye, "GRADISTAT: A Grain Size Distribution and Statistics Package for the Analysis of Unconsolidated Sediments," *Earth Surface Processes and Landforms* 26, no. 11 (2001): 1237–1248.

67. R. L. Folk and W. C. Ward, "Brazos River Bar [Texas]; a Study in the Significance of Grain Size Parameters," *Journal of Sedimentary Research* 27, no. 1 (1957): 3–26.

68. T. J. Weingartner, S. L. Danielson, R. A. Potter, et al., "Circulation and Water Properties in the Landfast Ice Zone of the Alaskan Beaufort Sea," *Continental Shelf Research* 148 (2017): 185–198.

69. F. K. Wiese, C. Ashjian, M. G. Asplin, et al., "Marine Arctic Ecosystem Study (MARES): Moorings on the Beaufort Sea shelf (2016–2018) and Program Synthesis," Anchorage (AK): US Department of the Interior, Bureau of Ocean Energy Management. OCS Study BOEM 2020-029, (2020): 286.

70. R. H. Herlinveaux and B. R. de Lange Boom, "Physical Oceanography of the Southeastern Beaufort Sea," Beaufort Sea Technical Report 18, (1975).

71. M. A. Janout, J. Hölemann, and T. Krumpen, "Cross-Shelf Transport of Warm and Saline Water in Response to sea ice Drift on the Laptev Sea Shelf," *Journal of Geophysical Research: Oceans* 118, no. 2 (2013): 563–576.

72. H. D. Pite, D. R. Topham, and B. J. van Hardenberg, "Laboratory Measurements of the Drag Force on a Family of two-Dimensional ice Keel Models in a Two-Layer Flow," *Journal of Physical Oceanography* 25, no. 12 (1995): 3008–3031.

73. E. C. Carmack and R. W. Macdonald, "Oceanography of the Canadian Shelf of the Beaufort Sea: A Setting for Marine Life," *Arctic* (2002): 29–45.

74. P. Lin, R. S. Pickart, D. B. Fissel, K. Borg, H. Melling, and F. K. Wiese, "On the Nature of Wind-Forced Upwelling and Downwelling in Mackenzie Canyon, Beaufort sea," *Progress in Oceanography* 198 (2021): 102674.

75. G. Tanski, L. Bröder, D. Wagner, et al., "Permafrost Carbon and CO2 Pathways Differ at Contrasting Coastal Erosion Sites in the Canadian Arctic," *Frontiers in Earth Science* 9 (2021): 207.

76. D. G. Lintern, R. W. Macdonald, S. M. Solomon, and H. Jakes, "Beaufort Sea Storm and Resuspension Modeling," *Journal of Marine Systems* 127 (2013): 14–25.

77. B. C. McDonald and C. P. Lewis, "Geomorphic and Sedimentologic Processes of Rivers and Coasts, Yukon Coastal Plain," Environ.-Soc. Comm. Northern Pipelines Task Force on Northern Oil Dev. (Rep. 73–79, 245 pp.). https://archive.org/details/31761114838881/page/252/mode/2up. (1973).

78. J. Falardeau, A. de Vernal, M. S. Seidenkrantz, et al., "Microfaunal Recording of Recent Environmental Changes in the Herschel Basin, Western Arctic Ocean," *Journal of Foraminiferal Research* 53, no. 1 (2023): 20–48.

Supporting Information

Additional supporting information can be found online in the Supporting Information section.